Quantum lens in an external electric field: Anomalous photoluminescence behavior

Arezky H. Rodríguez and C. Trallero-Giner[a)]
Department of Theoretical Physics, University of Havana, 10400 Havana, Cuba

(Received 10 September 2003; accepted 25 February 2004)

Electric field (**F**) effects in self-assembled quantum dots with a lens geometry have been studied. The optical selection rules and the origin of the anomalous behavior of the photoluminescence lines with the applied field reported by Raymond *et al.* [Phys. Rev. B **58**, R13415 (1998)] are analyzed in terms of the interband oscillator strength and lens symmetry. Also, an explicit analytical representation in the framework of the simple parabolic model for the electronic states as a function of **F** and lens parameter are given. The excitonic effect has been considered in the strongly confined regime when the excitonic Bohr radius is smaller than the dot dimensions. The influence of the lens geometry on the quantum Stark effect shows an asymmetric energy shift in the electron-hole transition. © *2004 American Institute of Physics.* [DOI: 10.1063/1.1710706]

I. INTRODUCTION

Discrete energy levels due to carrier confinement in semiconductor structures such as quantum wells, thin films, layered heterojunctions, and nowadays quantum dots (QD),[1,2] are of a great importance for the description of transport phenomena, electrical, and optical properties of these ''man-made'' systems. Quantum dot lasers are expected to have properties better than those of conventional quantum well lasers. The complete confinement in all three directions leads to a totally discrete energy spectrum with a noticeable increase in the density of states. Several works have been devoted to study, both experimentally and theoretically, the optical and electrical properties of quantum pyramids,[3–9] quantum disks,[10] spherical quantum dots,[11–13] and quantum lenses.[14–21] Also, experimental and theoretical studies when an external electric field is present have been performed in quantum wells,[22] quantum disks,[23] quantum pyramids,[24] cuboidal nanocrystal,[25] hemispherical quantum dots,[26] spherical quantum dots,[27–29] self-assembled quantum dots,[30–35] and with an arbitrary geometry.[36] These studies cover relevant topics such as electron and hole states, photoluminescence and photocurrent measurements.

Recently, an anomalous photoluminescence behavior has been reported (see Ref. 34). The photon emission lines of InAs/GaAs self-assembled quantum dots (SAQDs) under an external electric field F appear and disappear as the electric field is tuned. Several lines are clearly observed at low field, but they cannot be identified at higher fields. Moreover, the photoluminescence peaks that are identified at certain positive (negative) field, disappear for negative (positive) values. This article is addressed to this particular effect. We show that taking into account the full lens symmetry of the SAQD, the anomalous behavior of the emission lines can be explained qualitatively in terms of the interplay between the lens geometry and the mixing effect of the electron-hole wave functions when the external electric field is varied. The model also address the experimental observation reported in Refs. 31 and 32, of the electron-hole optical transition energies for SAQDs as a function of the electric field applied normal to the grown direction.

The article is organized as follows: Sec. II presents the mathematical model to deal with the confined Stark effect in a lens domain and Sec. III is devoted to the calculation of the oscillator strength and to the comparison with some experimental results. Finally, some conclusions are given in Sec. IV.

II. QUANTUM LENS IN AN ELECTRIC FIELD

A typical self-assembled quantum dot with lens symmetry presents a circular cross section of radio a and height b, as shown in the inset of Fig. 1(a). We consider an electron-hole pair confined in the SAQD domain under an electric field **F** parallel to its axial symmetry axis, taken as the z axis ($\mathbf{F}\|\hat{z}$). In the framework of the envelope function approximation, the exciton wave functions are taken as solutions of

$$\left[-\frac{\hbar^2}{2m_e^*}\nabla_e^2-\frac{\hbar^2}{2m_h^*}\nabla_h^2-e\mathbf{F}\cdot(\mathbf{r}_e'-\mathbf{r}_h')-\frac{e^2}{\kappa|\mathbf{r}_e'-\mathbf{r}_h'|}\right]\times\Psi_{\mathrm{eh}}(\mathbf{r}_e',\mathbf{r}_h')=(E-E_g)\Psi_{\mathrm{eh}}(\mathbf{r}_e',\mathbf{r}_h'),\tag{1}$$

where E_g is the gap energy, κ is the dielectric constant, and m_i^* and $\mathbf{r}_i'$ $(i=e,h)$ are the quasiparticle effective mass and its radius vector, respectively. As a first approximation, in the limit of strong spatial confinement ($a,b\ll$exciton Bohr radius a_B), the electron-hole Coulomb interaction can be considered as a perturbation. Neglecting the electron-hole correlation, the wave function $\Psi_{\mathrm{eh}}(\mathbf{r}_e',\mathbf{r}_h')$ is written in separable form by a product of electron and hole wave functions $\Psi_e(\mathbf{r}_e')\Psi_h(\mathbf{r}_h')$. According to the axial symmetry the one-particle wave function $\Psi_i(\mathbf{r}_i')$ in polar coordinates can be cast as

$$\Psi(r',\theta',\phi)=\frac{f(r',\theta')}{\sqrt{r'\sin\theta'}}\frac{\exp(im\phi)}{\sqrt{2\pi}}\tag{2}$$

a)Electronic mail: ctraller@ff.oc.uh.cu

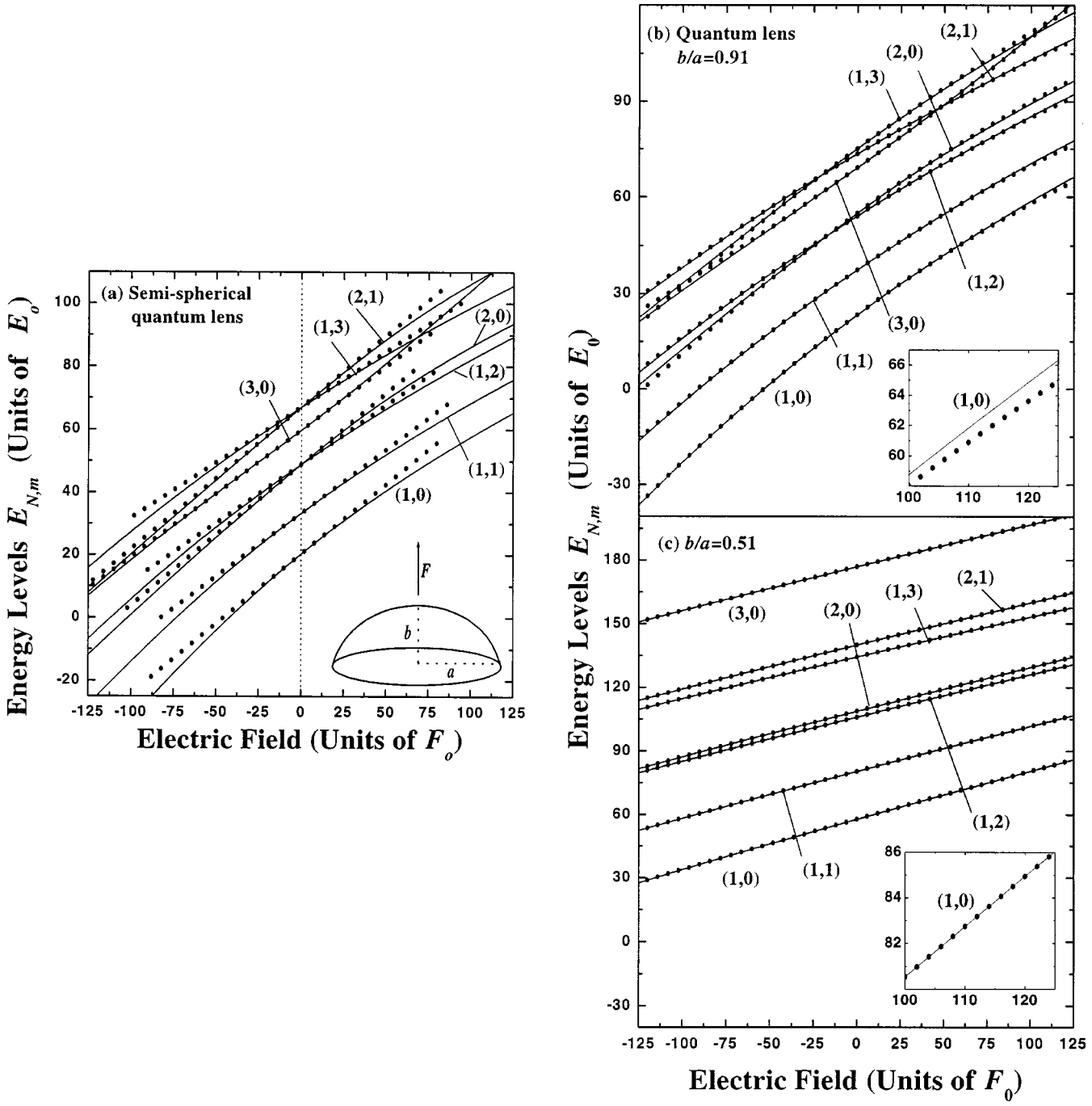

FIG. 1. First energy levels $E_{N,m}/E_0$ of a quantum lens as a function of the dimensionless electric field F/F_0. The (N, m) labels the levels by increasing energy for a given quantum number m. Solid lines correspond to the exact calculation. Dots represent the solution up to second order perturbation theory. (a) $b/a=1$ semispherical quantum lens. (b) Lens domain with $b/a=0.91$. (c) $b/a=0.51$. Inset (a) shows the QD lens symmetry. Insets (b) and (c) show the deviation for the ground state at high electric field between the exact results and perturbation theory.

with $m=0,\pm1,...$ being the z component of the orbital angular momentum and the function $f(r',\theta')$ satisfies the equation

$$-\frac{\hbar^2}{2m_i^*}\left(\nabla^2+\frac{m^2-1/4}{r'^2\sin^2\theta'}\right)f(r',\theta')$$
$$+\mathrm{sgn}(q)eFr'\cos\theta' f(r',\theta')=Ef(r',\theta'), \quad (3)$$

where $\mathrm{sgn}(q)=-e(e)$ for the electron (hole). In polar coordinates, $f(r',\theta')$ must fulfill the boundary condition at the lens boundary $\mathcal{C}$:

$$f(\mathcal{C})=0. \quad (4)$$

The Schrödinger Eq. (3) for a bidimensional quantum dot with lens-shape geometry in an electric field does not allow to find an explicit analytical closed solution for the wave functions $f(r',\theta')$. The lens geometry and the electric field break the spherical symmetry for which the square orbital angular momentum l and its z-component m are good quantum numbers. Closed solutions of Eq. (3) can be obtained if the lens domain is mapped into a semispherical one of radius a. This particular conformal mapping equation has

been reported in Ref. 20 and, according to Eq. (3) we obtain, in reduced variables, an equivalent equation defined in a semicircular domain given by

$$\left[-\nabla^2+(m^2-1/4)\frac{\mathcal{J}_\beta}{\chi_\beta^2}+\mathrm{sgn}(q)\sigma\xi\mathcal{J}_\beta Z_\beta\right]f^{(\beta,\xi)}(r,\theta)$$
$$=\sigma\lambda(\beta,\xi)\mathcal{J}_\beta f^{(\beta,\xi)}(r,\theta), \tag{5}$$

$$f(1,\theta)=0,\ \ f(r,\pi/2)=0. \tag{6}$$

In the earlier equation $\sigma=1(m_h^*/m_e^*)$ for electron (hole), $\xi=F/F_0$, $\lambda=E/E_0$, $F_0=E_0/(|e|a)$, $E_0=\hbar^2/(2m_e^*a^2)$, $\beta=b/a$, and the radius a was taken as a unit of length. The function Z_β is given by

$$Z_\beta(r,\theta)=\frac{2R^{\alpha/2}\sin(\alpha\phi)}{f_+^\alpha+f_-^\alpha+2R^{\alpha/2}\cos(\alpha\phi)} \tag{7}$$

and functions $\mathcal{J}_\beta(r,\theta)$, $\chi_\beta^2(r,\theta)$, $f_\pm$, R, α, and ϕ are defined in Ref. 20. It is worth to notice that Eq. (5) reduces to the semicircular case if $b/a=1$ with $\mathcal{J}_{\beta=1}=1$, $\chi_{\beta=1}=r\sin\theta$ and $Z_{\beta=1}=r\cos\theta$. At zero electric field ($\xi=0$) and $b/a=1$ the solutions of Eq. (5) are given by

$$f_{n,l,m}^{(0)}(r,\theta)=\sqrt{\sin\theta}P_l^{|m|}(\cos\theta)J_{l+1/2}(\mu_{n,l}r), \tag{8}$$

with $l=1,2,...,-l\leqslant m\leqslant l$, and $\mu_{n,l}$ is the nth zero of the Bessel function $J_{l+1/2}$. Since we have performed a conformal transformation, the Hilbert space of Eq. (3) at $F=0$ and $b/a=1$ is the same as that defined by Eq. (5) with $F\neq 0$ and $b/a\neq 1$. Hence, the set of functions (8) is a complete set of orthonormal eigenfunctions for the space of solutions determined by Eqs. (5) and (6). The boundary conditions (6) impose the restriction that $|l-m|=odd$ number. Therefore, we can search the wave function $f^{(\beta,\xi)}$, solution of Eq. (3), for each Hilbert subspace defined by the quantum number m, as a linear combination of the functions (8):

$$f_{N,m}^{(\beta,\xi)}(r,\theta)=\sum_{n,l}^{\infty}C_{n,l}^{(\beta,\xi)}(N,m)f_{n,l,m}^{(0)}(r,\theta). \tag{9}$$

Here, N enumerates, for a given values of m, the levels by increasing value of the energy $E_{N,m}$. Taking Eq. (9) in Eq. (5) leads to an infinite generalized eigenvalue problem for $\lambda_{N,m}(\beta,\xi)$ with eigenfunctions $\{C_{n,l}^{(\beta,\xi)}(N,m)\}$ for a given value of quantum number m. The corresponding matrix elements have to be evaluated numerically and standard numerical diagonalization techniques have been used to solve the system of equations. The electric field and quantum dot symmetry impose restrictive conditions on the energy levels, the carrier polarization, and the optical oscillator strength. These facts lead to a mixing of the wave functions (9) that should provide peculiar behaviors of the optical transitions.

A. Semispherical quantum lens

Let us first analyze the limit $b/a\to 1$. In the case of a spherical quantum dot the, states present $(2l+1)$-fold degeneracy. As the electric field is turned on the degeneracy is removed and the $l'=l\pm 1$ states with $\Delta m=0$ are mixed.[27] However, if the domain is reduced to a semispherical one, the solutions are restricted to those states fulfilling the condition $|l-m|=odd$ number with a degeneracy equal to l. The field keeps invariant the Hilbert subspaces for each value of $|m|$, remaining the twofold $(\pm m)$ degeneracy.

In Fig. 1(a) the first exact calculated electron energies $E_{N,m}$, for a semispherical quantum dot as a function of the dimensionless electric field F/F_0 are plotted (solid lines). The hole energies can be obtained by scaling the factor F/F_0 by $-(m_e^*/m_h^*)(F/F_0)$ and the factor E/E_0 by $(m_e^*/m_h^*)E/E_0$. At low electric fields an explicit expression can be derived for the carrier energy by applying perturbation theory in terms of the well known semispherical wave functions $|n,\ l,\ m\rangle$. Due to the constraint $|l-m|=odd$ number, the ground state $E_{1,0}$ at the semisphere corresponds to excited state $l=1$, $m=0$ in the spherical case.[27] It can be seen from Fig. 1(a) that the energy at $F\approx 0$ has a linear behavior with the applied electric field. At stronger fields the energy shifts are found to be proportional to F^2 in the lowest order of approximation. A good correspondence is observed between exact diagonalization and second order perturbation calculations for a certain range of the dimensionless electric field F/F_0. Our calculations show that, for an electron, the quadratic term obtained by the perturbation theory is two orders of magnitude lower than the linear term for a wide range of electric fields, while the energy levels have a strong quasistraight line behavior. Nevertheless, for hole states, and due to their mass value, a nonperturbative approach becomes necessary to describe the field effect on the quantum lens.

B. Nonsemispherical quantum lens

As the semispherical domain is deformed into a lens domain with circular cross section, the application of the electric field leads qualitatively to the same results, from the point of view of their symmetry properties, that in the semispherical case. Nevertheless, there is a strong concurrence between the lens deformation (confinement effect) and the energy provided by the external field. In Figs. 1(b) and 1(c) the electronic levels $E_{N,m}$ are shown as a function of the dimensionless electric field F/F_0 for two types of quantum lens $b/a=0.91$ [Fig. 1(b)] and 0.51 [Fig. 1(c)] representing a weak and strong lens confinement domain, respectively. Moreover, a perturbation theory calculation in terms of the applied electric field can be performed, but now the *eigenfunctions* $f_{N,m}^{(\beta,\xi=0)}$ and *eigenvalues* $\lambda_{N,m}(\beta)=E^{(\beta,\xi=0)}/E_0$ correspond to those defined in a *lens* domain with $b/a<1$. These wave functions have been previously reported in Ref. 35. For the sake of comparison, the calculated dimensionless energy values, following perturbation theory, are represented by dots in Figs. 1(b) and 1(c). We observe a good correspondence between exact and perturbation calculations obtained for both values of the lens domain here considered. Figures 1(b) and 1(c) show that the effect of the field on the energy decreases as b/a decreases, due to the increasing effect of the confinement, as it should be expected.

The probability density function (PDF) for the electron ground state $(N=1,m=0)$ and heavy hole states ($N=1$, 2, and 3 with $m=0$) for an InAs/GaAs SAQD with a lens domain is presented in Fig. 2 for three values of the applied electric field. It can be seen the stronger mobility of the hole with respect to the electron. Also, it is clear that for $F>0$

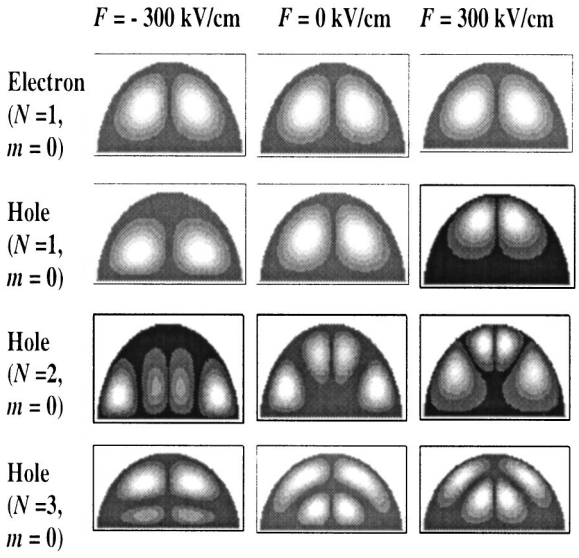

FIG. 2. Probability density function at $F=-300$, 0, and 300 kV/cm for the $(N_e=1,m=0)$ electron state and $(N_h=1,m=0)$, $(N_h=2,m=0)$, $(N_h=3,m=0)$ heavy hole states. For the calculation a ratio of $m_h^*/m_e^*=16.38$ was used.

$(F<0)$ the mean value of the heavy hole, $\langle f^{(\beta,\xi)}_{N_h,m}|z|f^{(\beta,\xi)}_{N_h,m}\rangle$, is located above (below) the electron one $\langle f^{(\beta,\xi)}_{N_e,m}|z|f^{(\beta,\xi)}_{N_e,m}\rangle$, and a nonsymmetric displacement with respect to $F=0$ is expected (see Fig. 3). Moreover, from the plot of the PDF we can see that the asymmetric behavior with respect the field $(F=\pm 300$ kV/cm) comes directly from the lens geometry.

Another important magnitude for the electro-optical properties is the carrier polarization, which is proportional to its z-component average. According to Eq. (9), and for a given state (N, m), this magnitude is given as follows:

$$\langle f^{(\beta,\xi)}_{N,m}|z'|f^{(\beta,\xi)}_{N,m}\rangle = a\sum_{n,l;n',l'} C^{(\beta,\xi)}_{n,l}(N,m)C^{(\beta,\xi)}_{n',l'}(N,m) \times\langle f^{(0)}_{n,l,m}|\mathcal{J}_\beta Z_\beta|f^{(0)}_{n',l',m}\rangle. \quad (10)$$

Figure 3 shows the behavior of $\langle z_i\rangle/a$ [$i=$electron (e), heavy (hh), and light (lh) holes] as a function of the dimensionless parameter F/F_0 for two quantum lens domains: (a) $b/a=0.91$ and (b) $b/a=0.51$. The states $(N=1,m=0)$ and $(N=2,m=0)$ have been considered for the calculation and the semiconductor parameters of Ref. 10 were used. From this figure, it can be seen that at $F=0$ the polarization is different from zero $(\langle z_i\rangle>0)$. This is a direct consequence of the lens symmetry, independent of the chosen Hamiltonian model, while the result $\langle z_e(F=0)\rangle=\langle z_h(F=0)\rangle$ is solely due to the assumed boundary conditions (4). As expected, in the framework of a homogeneous Hamiltonian mode, an opposite relative displacement of electrons and holes occurs along the direction of applied field. Also, the heavy hole quasiparticle is strongly affected by electric fields, reaching its asymptotic value, that is $\langle z\rangle/a\to b/a$ $(\langle z\rangle/a\to 0)$ for $F\to\infty$ $(F\to -\infty)$. From Figs. 3(a) and 3(b) it can be seen that as b/a decreases the polarization is less influenced by the field, and in the strong confinement regime lower values of $\langle z\rangle$ are reached.

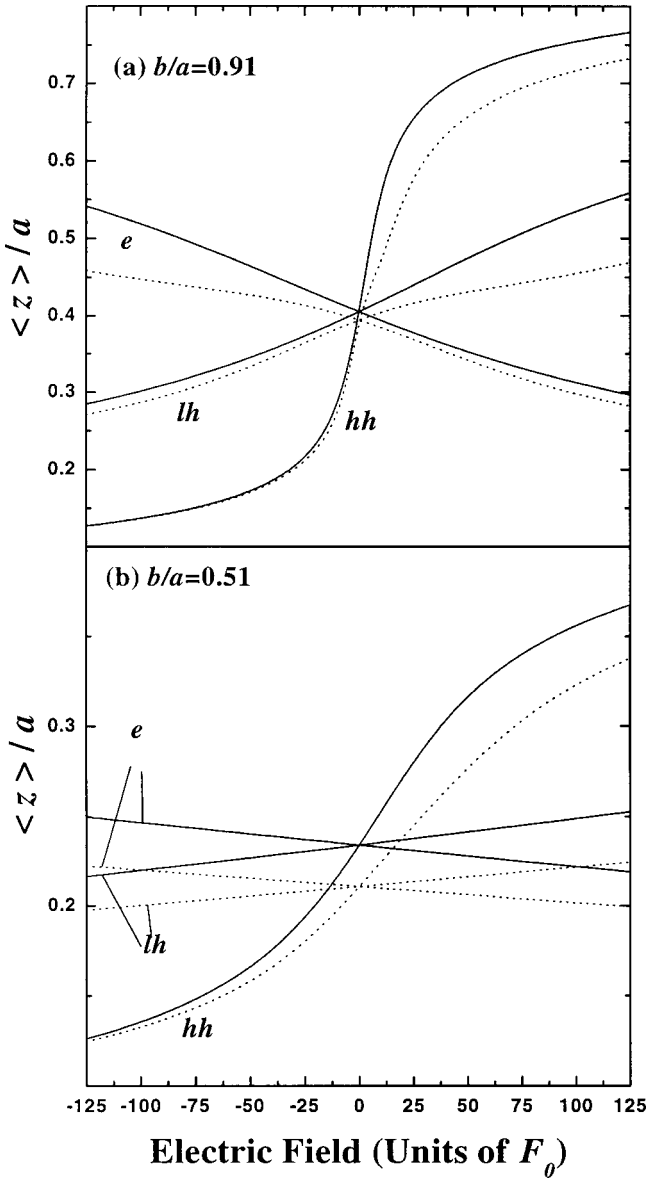

FIG. 3. Carrier polarization $\langle z\rangle$ in units of a as a function of the dimensionless electric field F/F_0 for the electrons (e), light (lh), and heavy (hh), holes. (a) Corresponds to a lens domain with $b/a=0.91$. (b) $b/a=0.51$. Solid lines represent the ground state $(N=1,m=0)$ and dotted lines to $(N=2,m=0)$ state.

C. Exciton correction

The Coulomb interaction can be taken as a perturbation if the strong confinement regime is considered. Thus, in the first order perturbation theory calculation the exciton correction can be cast as

$$\frac{\Delta E^{N_h,m_h}_{N_e,m_e}}{E_0}=\Lambda\int\frac{|\Psi_{N_e,m_e}(\mathbf{r}'_e)|^2|\Psi_{N_h,m_h}(\mathbf{r}'_h)|^2}{|\mathbf{r}'_e-\mathbf{r}'_h|}d\mathbf{r}'_e d\mathbf{r}'_h, \quad (11)$$

where $\mathbf{r}'_i$ is given in units of a, the integrals over $\mathbf{r}'_i$ are performed in the quantum lens domain (see the Appendix), and $\Lambda=2m_e^*e^2a/(\kappa\hbar^2)$ measures the ratio between the Coulomb and the spatial confined energies. In our calculation, the parameter Λ must be less than one. Figure 4 shows the excitonic binding energy as a function of the electric field. In

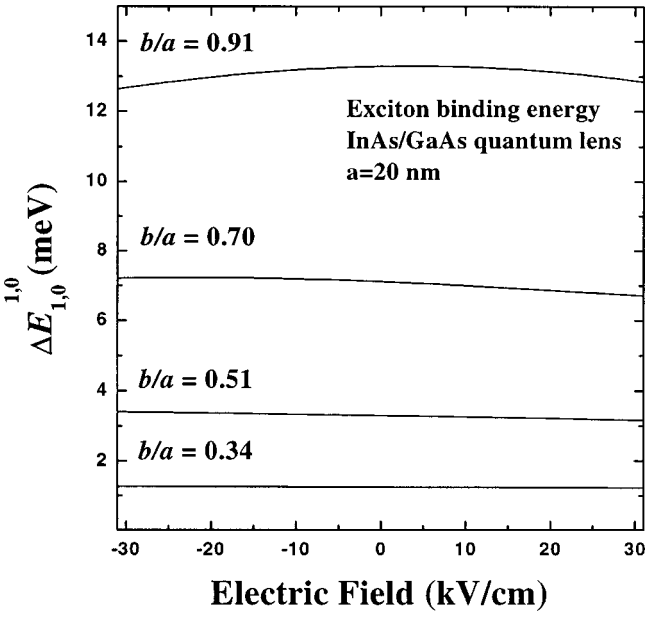

FIG. 4. Exciton binding energy of the ground state $\Delta E_{1,0}^{1,0}$ as a function of the electric field for some InAs/GaAs quantum lens: $b/a=0.91$, 0.70, 0.51, and 0.34.

the calculation, the values $a=20$ nm, $m_e^*=0.0152m_e$, $m_h^*=0.249m_e$, and $\kappa=10$ were used. From this figure it can be seen that the Coulomb interaction represents a small correction to the total electron-hole energy and ΔE will diminish as b/a decreases. Moreover, the influence of the electric field on the binding energy is practically negligible and can be considered as a constant. These facts are clearly understood due to the interplay between the spatial geometry interaction and the Coulomb and electric field ones.

III. OPTICAL MATRIX ELEMENT

In order to understand the origin of the photoemission lines as a function of **F**, we must calculate the interband optical matrix elements between different electron-hole pair states. In a first approach, and neglecting the Coulomb interaction, the interband optical matrix element is proportional to the oscillator strength of the electron-hole pair wave function $\Psi_{N_e,m_e;N_h,m_h}(\mathbf{r}_e',\mathbf{r}_h')$, given by

$$d^{(\beta,\xi)}(N_e,N_h;m)=\left|\int \Psi_{N_e,N_h,m}(\mathbf{r}',\mathbf{r}')d\mathbf{r}'\right|^2$$
$$=\left|\sum_{n,l;n'l'} C_{n,l}^{(\beta,\xi)}(N_e,m)C_{n',l'}^{(\beta,\xi)}(N_h,m)\right.$$
$$\left.\times\langle f_{n,l,m}^{(0)}|\mathcal{J}_\beta|f_{n',l',m}^{(0)}\rangle\right|^2. \quad (12)$$

In Fig. 5 it is shown the behavior of the oscillator strength $d^{(\beta,\xi)}$ for several electron-heavy hole states. The oscillator strength for the light hole behaves like a zoom of the heavy hole case near $F=0$, and it is not shown in the figures. Due to the infinite barriers model used, the oscillator strength is diagonal at $F=0$ and transitions between electrons and holes with different quantum numbers N, m are not allowed. The

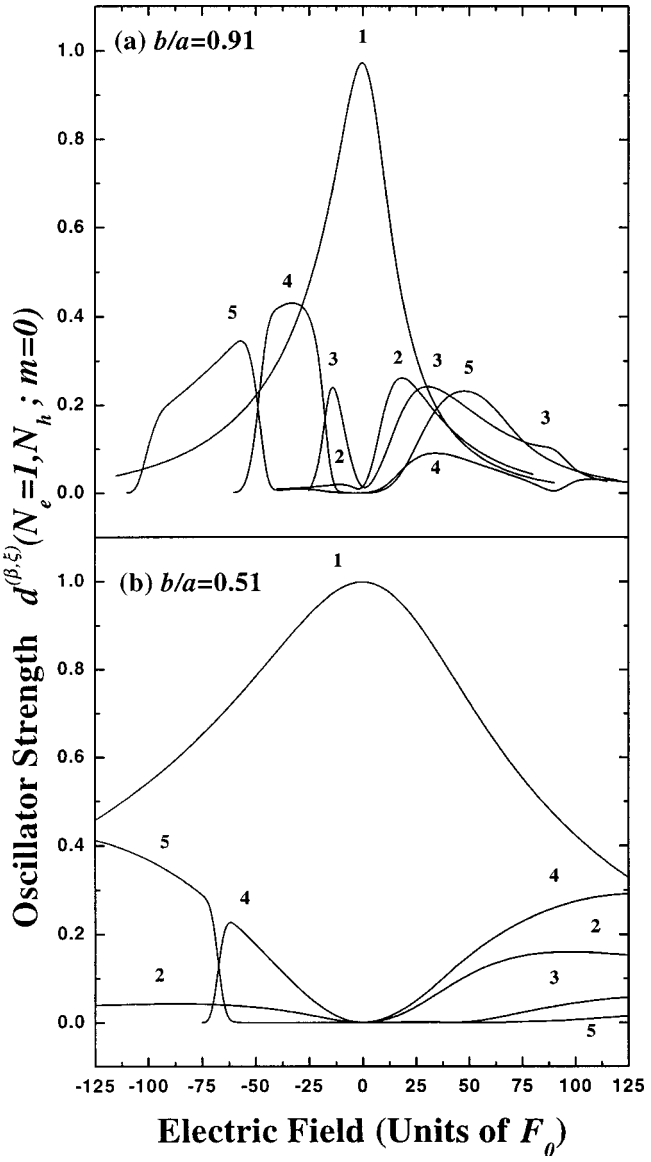

FIG. 5. Oscillator strength $d^{(\beta,\xi)}(N_e=1,N_h;m=0)$ as function of the electric field for five electron-hole transitions and two ratios of b/a. (a) $b/a=0.91$. (b) $b/a=0.51$. In the graphics the labels 1–5 represent the transitions from the heavy hole states $N_h=1$, 2, 3, 4, and 5 to the $N_e=1$ electron ground state, respectively.

electric field breaks this selection rule and transitions between states with different quantum numbers are allowed, provoking nondiagonal oscillator strengths different from zero. According to the dependence of the oscillator strengths $d^{(\beta,\xi)}$ on the electric field for $b/a=0.91$ [Fig. 5(a)], those transitions fulfilling the selection rule $\Delta m=m_e-m_h=0$ show a strong anisotropy with respect to $F=0$. This behavior is due to the lens geometry, i.e., the electron/hole motion in the z direction is different with respect to the positive or negative direction of the field. Another interesting feature in Fig. 5 is the appearance and disappearance of electron-hole transitions as the electric field is tuned. For example, the transition 2 [heavy hole state (2,0) to electron state (1,0)] at $F/F_0=15$ shows a maximum in the oscillator strength, while at negative field this emission line has practically zero intensity. The opposite can be argued for the oscillator strength 4

[transition from the heavy hole state (4,0) to electron state (1,0)], where the stronger maximum is located at negative field and a very weak photoluminescence lines are predicted at $F/F_0>0$. A similar symmetric behavior of the emission lines with respect the applied electric field is observed for the transitions 1, 3, and 5. This nonmonotonic dependence of the photoluminescence lines on F is explained by the admixture of states with different orbital quantum number l induced by the electric field and the lens geometry. The field breaks the spatial parity of the final function $f^{(\beta,\xi)}$ in such a way that all components $C_{n,l}^{(\beta,\xi)}$ in Eq. (9) contribute to the new state. At $F=0$ and due to the restriction $|l-m|=odd$ number, the optical transition $\langle f_{N_e=1,0}^{(\beta,\xi=0)}|f_{N_h,0}^{(\beta,\xi=0)}\rangle=0$ for $N_h=2,3,...$ The field couples states with different angular momentum l and the coefficients $C_{n,l}^{(\beta,\xi)}$ for $l=even$ number are different from zero, allowing optical transitions between heavy and electron wave functions with different quantum number N and $m=0$. Moreover, following Eqs. (5) and (9), the weights $C_{n,l}^{(\beta,\xi)}$ are nonsymmetric with respect to the direction of F. This behavior is clearly observed in the $E_{N,m}$ energy dispersion shown in Fig. 1, providing an evidence of the strong admixture in the wave functions $f_{N,0}^{(\beta,\xi)}$. Therefore, anomalous variations of the oscillator strength and of in the photoluminescence spectra, as a function of the electric field, are expected.

Regarding to excitonic effects, it is necessary to point out that within the strong confinement limit $(a,b\ll a_B)$, the behavior of the oscillator strength $d^{(\beta,\xi)}(N_e=1,N_h;m=0)$ as a function of the electric field and the quantum lens geometry parameter b/a do not change at all. The main characteristics detailed in Fig. 5, and those reported in Ref. 34 are linked to the spatial symmetry properties. The electron-hole attractive correlation is responsible for a small increase of that particular transition (a more bright line in the photoluminescence spectrum), but it will not introduce a different spectral intensity distribution as a function of F. This spectral distribution is determined by the fact that the lens shape geometry and the electric field reduce the spherical symmetry of the Coulomb potential, leading to a specific admixture of states for the optical transitions.

It is useful to analyze, qualitatively and quantitative, the results provided by the simple electronic model here considered, with the experimental observations. Electron-hole optical transitions energies for SAQDs as a function of the field normal to the grown direction have been reported in Refs. 31, 32, 34, and 37, showing a clear asymmetric Stark shift. In order to fit the obtained experimental data, several models have been proposed. For example, in Ref. 34 effective potentials for electron and holes were assumed, while in Refs. 31 and 32 an effective pyramidal geometry (severely truncated) is considered. Nevertheless, in our opinion, there is still some uncertainty about the fundamental parameters which lead to the mentioned asymmetric Stark shift. Let us first analyze qualitatively the influence of the lens domain on the Stark effect. In our case of a SAQD with lens geometry, the electronic energy shows an asymmetric Stark shift due to the linear dependence on F (see Fig. 1). Hence, the allowed optical electron-hole transition energy has a permanent dipole proportional to $P_d=\langle i_e|\mathcal{J}_\beta Z_\beta|i_e\rangle-\langle i_h|\mathcal{J}_\beta Z_\beta|i_h\rangle$. In general, any theoretical formalism which provides different probability density distributions for electrons and holes will lead to a permanent nonzero intrinsic dipole in the quantum dot. This can be achieved including finite barriers potentials, using any extended $k\cdot p$ Hamiltonian model or taking into consideration different strain distributions for electrons and holes. The fundamental issue is to get a value for P_d in agreement with the experimental value. The model presented in Sec. II, which considers infinite barriers and neglects the (not well known) strain distribution, can reproduce the order of magnitude and the curvature of the measured transition energy with respect to the applied electric field. Figure 6 shows the dependence of the ground state transition energy on F, measured by photocurrent technique,[31,32] for a QD with a base size of 18 nm in diameter and height of 8.5 nm. Here we compare several theoretical fittings, according to the model of Sec. II, where the solid line represents the excitonic transition and the dotted lines the same result using perturbation theory without excitonic effect. In the calculation the best fittings have been obtained with the set of values $m_e^*=0.015m_e$, $m_h^*=0.249m_e$, and $E_{\text{gap}}(T=200\text{ K})=0.348$ eV.[38] The wave function penetration into adjacent environment is considered by a fitting procedure to reproduce the data reported in Ref. 31. In our case, we obtain and effective radius $a_{\text{eff}}=8.5$ nm. In some extent, the values of the electron and holes masses used include phenomenologically the strain field distribution on the band structure.[4,5] The excitonic correction has been calculated according to Eq. (11). The resulting binding energy calculation for the ground

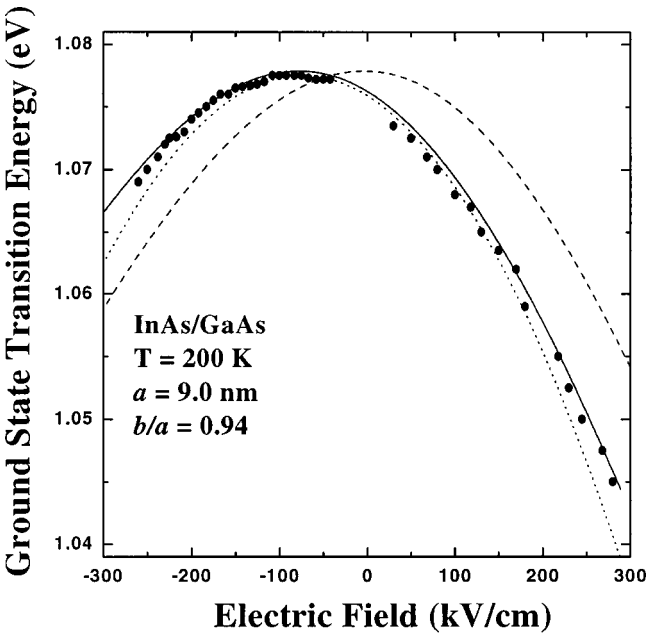

FIG. 6. Exciton ground state transition energy as a function of the electric field F for a QD with lens geometry of a radius $a=9$ nm and height $b=8.5$ nm. Dots represent the data from Ref. 31, solid line is the exact calculation including excitonic effect and dotted lines are the Rayleight–Schrödinger second order perturbation theory. A field $F_i=-74$ kV/cm has been introduced in order to shift rigidly the theoretical calculation to compare with the experimental data. Dashed lines correspond to the exact calculation with $F_i=0$ kV/cm.

state $\Delta E^{(\mathrm{exc})}$ at $F=0$ is equal to 24.9 meV and $\Delta E^{(\mathrm{exc})}=24.6$, 23.8 meV at $F=\pm 290$ kV/cm. When a lens geometry is assumed, the optical ground state transition energy calculation presents an asymmetric Stark shift with respect to $F=0$, as can be seen in the Fig. 6. This asymmetry comes out from the lens geometry and the difference between the electron and hole masses. Since we are interested in analyze the influence of the lens geometry on the Stark effect, a built-in electric field $F_i=-74$ kV/cm was added *ad hoc*, shifting rigidly the theoretical calculations. It can be seen that the principal features, as the order of magnitude, curvature, and asymmetry, are well reproduced by the quantum lens model. Concerning the internal field F_i, we should mention that its origin is very controversial. In Ref. 34, the value of F_i is mainly due to a strong increase in the electric confinement energy, as the external field forces the electron towards the apex of the dot. In Ref. 31, the internal field is obtained by a graded Ga composition in the dot and the correct direction of the permanent dipole is reached by a severe truncation of the QD, modeled as a pyramid. It is important to recall that the presence of an internal field has been reported or wurtzite CdSe spherical QDs.[2] This work propose the possibility of facets on the QD surface and/or surface traps, supporting the departure from the symmetrical shapes.

Using the same set of parameters employed in the Fig. 6, we compare in Fig. 7(a) the oscillator strength dependence on F for the ground state (solid line) with the experimental observations (dots).[31] The observed maximum occurs at $F=-140$ kV/cm, while in the calculation the maximum is located at $F=-74$ kV/cm, in correspondence with the fittings shown in Fig. 6. Nevertheless, we can see good agreement between the experimental results and the calculations. Accordingly, the behavior of the first excited state as a function of the applied electric field is shown in Fig. 6(b). The theoretical calculations correspond to the $(N_e=1,m=0)\Rightarrow(N_h=2,m=0)$ and $(N_e=1,m=0)\Rightarrow(N_h=3,m=0)$ excitonic transitions and are represented by solid lines while the experimental data are depicted by dots. The obtained results indicate that the first observed excited state should be a combination of several optical transitions. In panel 6(c), we compare our results for the ground state transition energy for a QD of radius $a=7.5$ nm, $b=3.5$ nm, and ratio of $b/a=0.47$ with the data reported in Ref. 31. In this case, the strong confinement provokes a larger penetration of electrons and holes into the surrounding medium. In order to take into account this effect we introduce an effective quantum lens of radius $a_{\mathrm{eff}}=15.16$ nm keeping the same ratio $b/a=0.47$. This procedure had been used in the past to simulate the finite potential barrier model,[22,39,40] and represents an alternative to include the finite barrier band offset avoiding its mathematical complications. In the present calculation the values of m_e^* and m_h^* are the same employed in the fittings of Fig. 6 but now a built-in internal field $F_i=-80$ kV/cm was assumed. Also, in the figure the second order perturbation approach (dotted lines) is shown, evidencing the good correspondence with the exact calculation.

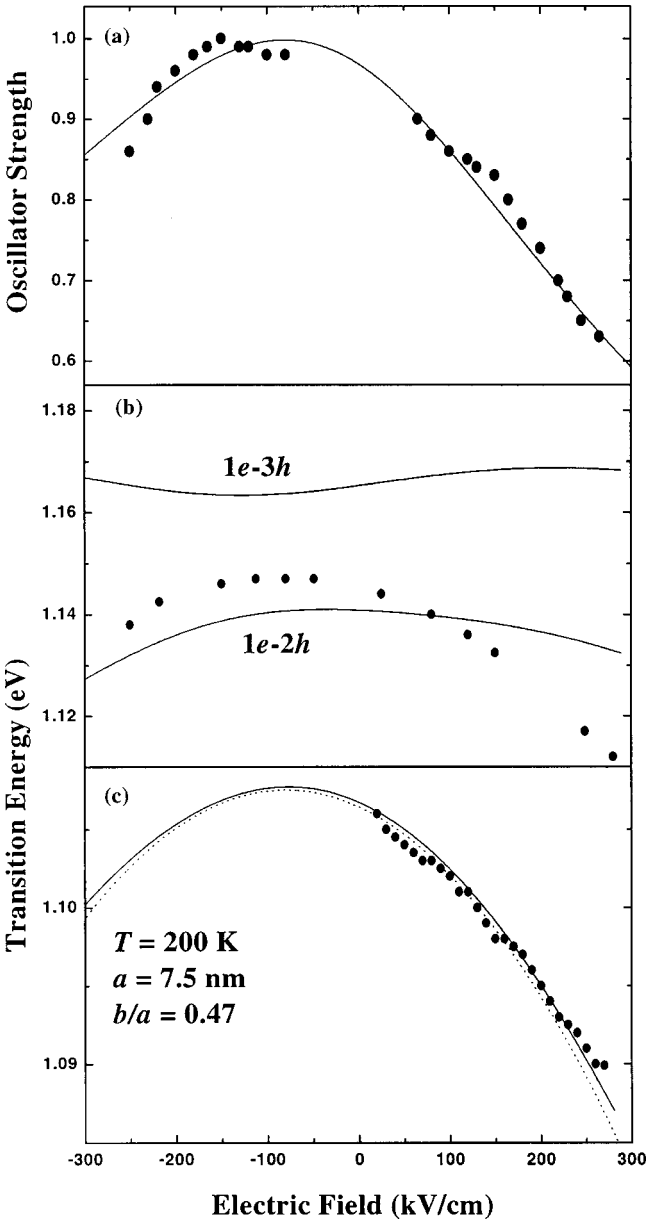

FIG. 7. (a) Ground state oscillator strength as function of the electric field for the sample of Fig. 6. (b) First measured exited state energy according to Ref. 31. In the calculation the set of parameters of Fig. 6 has been employed. Solid lines represent calculation for the $1e-2h$ and $1e-3h$ excitonic states. (c) Ground state transition energy as a function of the electric field F for an InAs/GaAs quantum lens geometry of a radio $a=7.5$ nm and $b/a=0.47$. In the calculation and effective radius of $a_{\mathrm{eff}}=15.16$ nm has been used. In all graphics the experimental data are represented by dots, the exact calculation by solid lines, and dotted lines are the Rayleigh–Schrödinger second order perturbation theory.

IV. CONCLUSIONS

We have shown that self-assembled quantum dots with lens geometry lead to peculiar oscillator strength distribution as a function of **F**. The mixing of different electronic states due to the interplay between lens deformation and the field, explains the appearance and disappearance of the photoluminescence lines as the electric field is tuned. Also it is shown that the lens symmetry conduces to an asymmetric Stark

shift. The main experimental features observed of the quantum Stark effect in self-organized quantum dots can be explained by assuming a lens geometry.

Finally, we have reported an analytical representation for the electronic states of the dot as function of the lens geometry and the electric field normal to the dot plane. We have not considered the stress and the Ga distribution in the dot. However, the reported representation for the eigensolutions could provide a basis to incorporate such effects and to go more deeply into the evolution of the optical properties on the external applied fields.

ACKNOWLEDGMENTS

C.T-G. is grateful to A. M. Alcalde and S. García for helpful discussions and carefully reading of the manuscript.

APPENDIX

Using the identity[41]

$$\frac{1}{|\mathbf{r}_e'-\mathbf{r}_h'|}=4\pi\sum_{p=0}^{\infty}\sum_{s=-p}^{s=p}\frac{1}{2p+1}\frac{r_<'^p}{r_>'^{p+1}}\times Y_{p,s}^*(\theta_e',\phi_e')Y_{p,s}(\theta_h',\phi_h') \tag{A1}$$

and Eq. (2) we obtain

$$\Delta E_{N_e,m_e}^{N_h,m_h}=2E_0\Lambda\sum_{p=0}^{\infty}\frac{I_p(\beta,\xi)}{2p+1}, \tag{A2}$$

where

$$I_p(\beta,\xi)=\sum_{i,j,i',j'}^{\infty}C_i^{(\beta,\xi)}(N_e,m_e)C_j^{(\beta,\xi)}(N_h,m_h)s\times C_{i'}^{(\beta,\xi)}(N_e,m_e)C_{j'}^{(\beta,\xi)}(N_h,m_h)\mathcal{I}_{i,j,i',j'}(p) \tag{A3}$$

and

$$\mathcal{I}_{i,j,i',j'}(p)=\int d\mathbf{r}_e'd\mathbf{r}_h'f_{i,m_e}^{(0)}(r_e',\theta_e')f_{j,m_h}^{(0)}(r_h',\theta_h')\times\frac{r_<'^p}{r_>'^{p+1}}P_p(\cos\theta_e')P_p(\cos\theta_h')\times f_{i',m_e}^{(0)}(r_e',\theta_e')f_{j',m_h}^{(0)}(r_h',\theta_h'). \tag{A4}$$

In the earlier equation i labels the set of quantum number (n, l) and the variables r', θ' are function of r, θ coordinates according to the inverse of the mapping transformation between the lens geometry and the semispherical domain.[20] The integrals $\mathcal{I}$ is over the two-dimensional lens domain and were performed numerically following a Monte Carlo procedure. These integrals solely depend on lens deformation b/a and are independent on the electric field.

[1] D. Bimberg, M. Grundmann, and N. N. Ledentsov, *The Quantum Dot Heterostructures* (Wiley, Chichester, 1999).
[2] A. D. Yoffe, Adv. Phys. **50**, 1 (2001).
[3] M. A. Cusack, P. R. Briddon, and M. Jaros, Phys. Rev. B **54**, R2300 (1996).
[4] M. A. Cusack, P. R. Briddon, and M. Jaros, Phys. Rev. B **56**, 4047 (1997).
[5] M. Grundmann, O. Stier, and D. Bimberg, Phys. Rev. B **52**, 11969 (1995).
[6] L. Wang and A. Zunger, Phys. Rev. B **59**, 15806 (1999).
[7] C. Pryor, Phys. Rev. B **57**, 7190 (1998).
[8] O. Stier, M. Grundmann, and D. Bimberg, Phys. Rev. B **59**, 5688 (1999).
[9] A. Zunger, Phys. Status Solidi B **224**, 727 (2001).
[10] E. Menéndez-Proupin, C. Trallero-Giner, and S. E. Ulloa, Phys. Rev. B **60**, 16747 (1999).
[11] J. L. Marín, R. Riera, and S. A. Cruz, J. Phys.: Condens. Matter **10**, 1349 (1998).
[12] E. Menéndez, C. Trallero-Giner, and M. Cardona, Phys. Status Solidi B **199**, 81 (1997).
[13] T. Uozumi *et al.*, Phys. Rev. B **59**, 9826 (1999).
[14] D. J. Eaglesham and M. Cerullo, Phys. Rev. Lett. **64**, 1943 (1990).
[15] A. Forchel *et al.*, Semicond. Sci. Technol. **11**, 1529 (1996).
[16] I. Hapke-Wurst *et al.*, Semicond. Sci. Technol. **14**, L41 (1999).
[17] J. H. Zhu, K. Brunner, and G. Abstreiter, Appl. Phys. Lett. **72**, 424 (1998).
[18] X. Z. Liao *et al.*, Phys. Rev. B **58**, R4235 (1998).
[19] J. M. Moison *et al.*, Appl. Phys. Lett. **64**, 196 (1994).
[20] A. H. Rodríguez, C. Trallero-Giner, S. E. Ulloa, and J. Marín-Antuña, Phys. Rev. B **63**, 125319 (2001).
[21] J. Zou, X. Z. Liao, D. J. H. Cockayne, and R. Leon, Phys. Rev. B **59**, 12279 (1999).
[22] C. Trallero-Giner and J. López-Gondar, Physica B **138B**, 287 (1986).
[23] E. C. Niculescu, Phys. Status Solidi B **226**, 385 (2001).
[24] C. M. A. Kapteyn *et al.*, Phys. Rev. B **60**, 14265 (1999).
[25] D. A. B. Miller, D. S. Chemla, and S. Schmitt-Rink, Appl. Phys. Lett. **52**, 2154 (1988).
[26] E. B. Salem, S. Jaziri, and R. Bennaceur, Phys. Status Solidi B **224**, 397 (2001).
[27] E. Casado and C. Trallero-Giner, Phys. Status Solidi B **196**, 335 (1996).
[28] H. Rossmann, A. Schülzgen, F. Henneberger, and M. Müller, Phys. Status Solidi B **159**, 287 (1990).
[29] S. Nomura and T. Kobayashi, Solid State Commun. **73**, 425 (1990).
[30] V. Davydov *et al.*, Phys. Status Solidi B **224**, 425 (2001).
[31] P. W. Fry *et al.*, Phys. Rev. Lett. **84**, 733 (2000).
[32] P. W. Fry *et al.*, Phys. Status Solidi B **224**, 497 (2001).
[33] I. Shtrichman *et al.*, Phys. Rev. B **65**, 081303 (2002).
[34] S. Raymond *et al.*, Phys. Rev. B **58**, R13415 (1998).
[35] A. H. Rodríguez and C. Trallero-Giner, Phys. Status Solidi B **230**, 463 (2002).
[36] A. A. Kiselev, K. W. Kim, and M. A. Stroscio, Phys. Rev. B **60**, 7748 (1999).
[37] W. Sheng and J. P. Leburton, Phys. Rev. Lett. **88**, 167401 (2002).
[38] *Landolt-Börnstein Tables, Numerical Data and Functional Relationships in Science and Technology*, edited by O. Madelung (Springer, Berlin, 1982), Vol. 17a.
[39] D. A. B. Miller *et al.*, Phys. Rev. Lett. **53**, 2173 (1984).
[40] M. Matsuura and T. Kamizato, Phys. Rev. B **33**, 8385 (1986).
[41] J. D. Jackson, *Classical Electrodynamics* (Wiley, 1999, New York, 1999).